JOURNAL OF AIRCRAFT
Vol. 37, No. 5, September–October 2000

Response of Selected Integrally Stiffened Curved Aluminum Panels Subjected to Combined Loads

Dawn C. Jegley*
NASA Langley Research Center, Hampton, Virginia 23681-2199

The results of an analytical and experimental study of integrally stiffened curved aluminum panels are presented. A panel was tested and analyzed by applying an axial compressive load. The boundary and loading conditions for the panel were varied analytically to determine their effects on panel response. Elements representing clips between frames and longerons were added to evaluate the effect of these clips on the deformations of the panel. Panels were analyzed using a nonlinear finite element analysis. Axial compressive and internal pressure loads were analytically applied as individual loads and as combined loads. Strains and displacements, including the rotation of longerons, are compared.

Introduction

ONE of NASA's goals is to reduce the cost of air travel by 50% in the next 20 years. To achieve this cost reduction, NASA is assisting in the development of the technology needed for future low-cost, lightweight structures for commercial transport aircraft. The manufacturing of current aircraft is a labor intensive and expensive process. One way to reduce the labor required and, therefore, the expense, is to fabricate large parts of a structure from a single piece of metal and minimize the large number of different parts and fasterners. By machining skin, longerons, and flanges from a single piece of aluminum, many fasteners and many hours of labor are eliminated. One such panel was examined in this study.

Panel Description

A stiffened test panel was fabricated from 1.5-in.-thick (3.81 cm) 7050-T7451 aluminum plate stock. The panel was machined to the desired dimensions first as a flat panel with four Z-stiffener longerons in the axial direction. The longerons were spaced 8 in. (20.3 cm) apart and were integrally attached to the skin. After the skin and Z-stiffeners were trimmed to the desired dimensions, the panel was shaped to the desired radius. Frames were riveted to the skin at locations 6 in. (15.2 cm) from the top and bottom edges of the panel. A photograph of the panel is shown in Fig. 1.

The panel is 32 in. (0.813 m) long and approximately 32 in. wide. It has a radius of 118.5 in. (3.0 m) to the center of the skin thickness. The panel skin is nominally 0.06 in. (0.152 cm) thick in the thinner regions and 0.17 in. (0.432 cm) thick in the thicker regions. Thick-skin regions behave like the skin plus flanges for the longerons and provide additional stiffness at the frame locations. Longerons are 1.22-in.-tall (3.10 cm) Z-shape stiffeners, which have a 0.08-in.-thick (0.203 cm) web and a 0.12-in.-thick (0.305 cm) cap. Frames are 5.5 in. (14.0 cm) tall and have a 0.08-in.-thick web and a 0.12-in.-thick cap. Dimensions of these elements are shown in Fig. 2. No attachments between the frames and the longerons are used. The longerons pass through openings in the frames (referred to herein as "mouseholes"), as shown in Fig. 1.

Loading Conditions and Instrumentation

The test panel was loaded in axial compression. The loaded edges of the panel were ground flat and parallel before loading. The edges of the panel were placed against the test machine platens with no potting or other support. No edge support or other lateral supports were used. The panel was instrumented with strain gauges and direct-current displacement transducers, which were used to monitor end-shortening and out-of-plane displacement. Moiré interferometry was also used to monitor out-of-plane displacements of the panel skin. The panel was loaded to failure at a rate of approximately 10,000 lb/min (44 kN/min).

Strain gauges were located 2 in. (5.08 cm) from the top of the panel and along the panel axial centerline, as shown in Fig. 1. Back-to-back axial strain gauges were placed on the skin midway between the longerons. Axial strain gauges were placed on the top of each longeron and on the skin opposite the longeron. Back-to-back lateral strain gauges were placed on the longeron webs to monitor rolling of the longerons.

Analysis

A nonlinear finite element analysis using the STAGS[1] computer code was conducted to evaluate the behavior of the test panel and to examine the effect of various boundary conditions on the panel response. The finite element model is shown in Fig. 3. The model has approximately 40,000 degrees of freedom. Quadrilateral, four-noded plate elements were used to model all parts of the panel. A more complete description of the element used is presented in Ref. 2. Details of modeling and nonlinear analysis formulations used in STAGS are found in Refs. 3 and 4. An example of postbuckling analysis and modeling using STAGS is presented in Ref. 5. In the analysis of this panel, offsets are used in the thick-skin regions to shift nodal locations so that eccentricities in the panel are accurately included in the model. The material is assumed to be isotropic with a Young's modulus of 10.7×10^6 psi and a Poisson's ratio of 0.3.

In analyzing the test panel, the unloaded edges are assumed to be unsupported while rotations and out-of-plane motion of the loaded edges are not permitted. Lateral motion is restricted only at the center of the skin at each end of the panel. End-shortening is required to be uniform across the loaded edge of the panel.

The analysis of the test panel was conducted in two steps. First, the panel was analyzed by assuming that no initial geometric imperfections were present. A linear bifurcation buckling analysis of the perfect panel was conducted. The buckling analysis indicated that there were numerous buckling loads with several different mode shapes occurring at very low loads. A geometrically nonlinear analysis of the perfect panel was conducted that would accurately account for changes in deformation shapes as the applied load was increased. Loaded-edge boundary conditions were considered in which all rotations and out-of plane deformations were assumed to be zero and in which only the out-of-plane deformations were assumed to be zero. However, numerical difficulties in the form of an inability to obtain a converged solution even with extremely small load steps

Received 4 May 1999; revision received 4 December 1999; accepted for publication 11 December 1999.

*Senior Aerospace Engineer, MS 190, Mechanics and Durability Branch, Structures and Materials Competency. Senior Member AIAA.

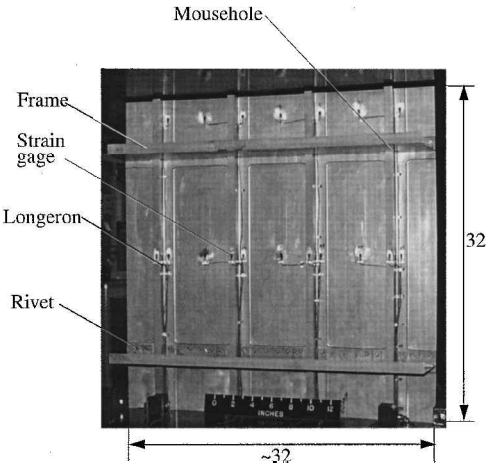

Fig. 1 Panel prior to testing (dimensions are in inches).

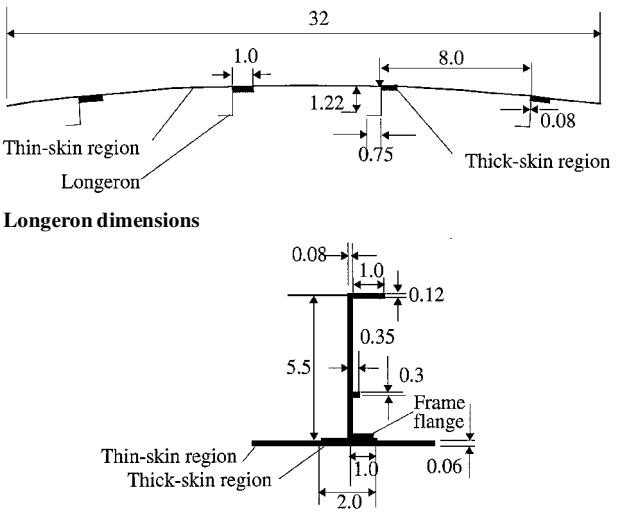

Fig. 2 Panel geometry (dimensions are in inches).

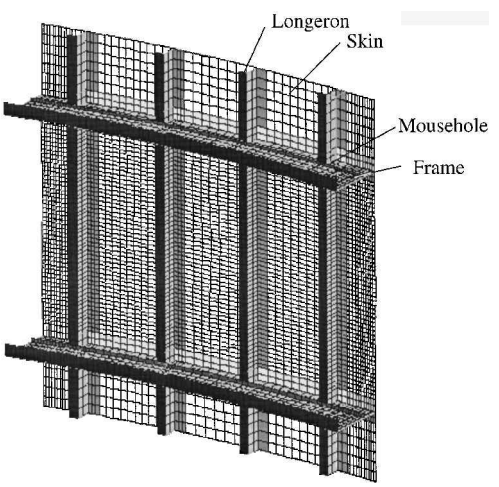

Fig. 3 Finite element model.

made it difficult, if not impossible, to obtain results for loads greater than approximately half of the failure load of the panel for either of these boundary conditions. To obtain predictions for greater load levels, initial imperfections with magnitude 0.1 in. (0.254 cm) were added. These assumed imperfections had the approximate deformation shape predicted by the nonlinear analysis of the perfect panel. These imperfections were included only in the thin-skin regions of the panel between the frames. A geometrically nonlinear analysis of the imperfect panel was conducted, including the initial imperfections in the analysis, which significantly reduced the amount of time needed to analyze the panel and the number of incremental load steps needed to obtain results.

The imperfect panel loaded in axial compression was analyzed using three sets of boundary conditions. The assumed boundary conditions for the loaded edges were the following: 1) rotations and out-of-plane motion of the panel skin and longerons were restrained; 2) out-of-plane motion of the panel skin and longerons were restrained; and 3) out-of-plane motion of the panel skin was restrained. Numerical analyses for loads up to 66,000, 100,000, and 89,000 lb (293, 444, and 395 kN) were performed for the three types of boundaries, respectively. In some cases numerical difficulties caused by lack of convergence prevented analysis from being conducted for higher load levels.

One additional restraint condition was considered. Two connections between the frames and longerons at each mousehole were added to simulate the presence of clips that would prevent independent rotation of the longerons and frames. Only the boundary condition that restrained out-of-plane motion of the panel skin and the longerons at the loaded edges was considered for the analysis of the panel with longeron-to-frame connections.

A pressure load condition was also included by applying a normal load in the out-of-plane direction to the concave surface of the panel skin. Pressure loads on each element were determined by the element area so that the skin was uniformly loaded. Panels with and without longeron-to-frame connections were analyzed. Pressure loads up to 18 psi without axial compressive load and pressure loads of 9 psi with axial compressive loads up to 74,000 lb (329 kN) were applied.

Results

Analytical and experimental results are presented first for axial compressive load alone. Then analytical results are presented for a pressure load applied to the skin. Finally, analytical results are presented for the panel subjected to a combination of compression and pressure loads. Results are also presented for geometrically perfect and geometrically imperfect panels. Except where otherwise noted, results shown are for analyses with the loaded-end boundary conditions that restrain out-of-plane deformation everywhere on the loaded edges, but free rotations in the skin and longerons are allowed. Because little effect is seen for variations in boundary conditions on the loaded edges, additional results are not presented in detail. In graphical comparisons between experimental and analytical results, experimental results are shown as solid lines, and analytical results are shown as dashed lines.

Axial Compression

Experimental results indicate that the panel skin has a nonlinear response. Changes in Moiré patterns of the panel skin during loading indicate that the panel buckled in the outer thin-skin regions at a load of less than 10,000 lb (44 kN). The loading of the test panel was continued past buckling, and the panel continued to support an increased axial load to a maximum load of 97,200 lb (432 kN). Photographs of the panel showing out-of-plane deformation patterns at loads of 18,000, 44,000, and 85,000 lb (80, 196, and 378 kN) are shown in Fig. 4. Loading was continued until increasing the end displacement no longer increased the load. The attempt to increase the load further resulted in increased displacement and strain, but no increase in load. An example of this increased strain is shown in Fig. 5a for two strain gauges on the axial centerline of the panel. The strain gauge on the skin measured large strains as the displacement was continued past the point of maximum load. No cracking in any part of the panel was observed. No rivets appeared to be damaged. This maximum load of 97,200 lb (432 kN) corresponds to a global stress of approximately 30,100 lb/in^2 (207,540 kPa). Permanent deformation was present in the panel after failure. This permanent deformation is shown in Fig. 5b. Because plasticity is not included in the analysis, test results presented in the subsequent figures are limited to loads that are less than the maximum experimental load.

Analysis of the geometrically perfect panel predicts buckling loads of 8062 and 8095 lb (35.8 and 36.0 kN) with loaded-end

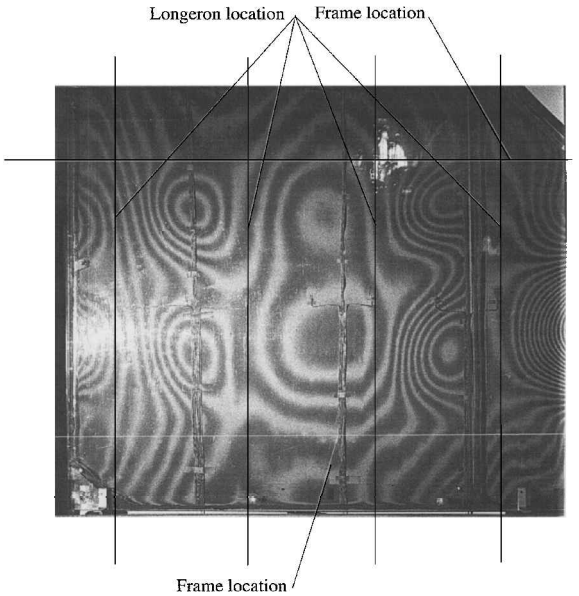

a) Applied compressive load of 18,000 lb (80 kN)

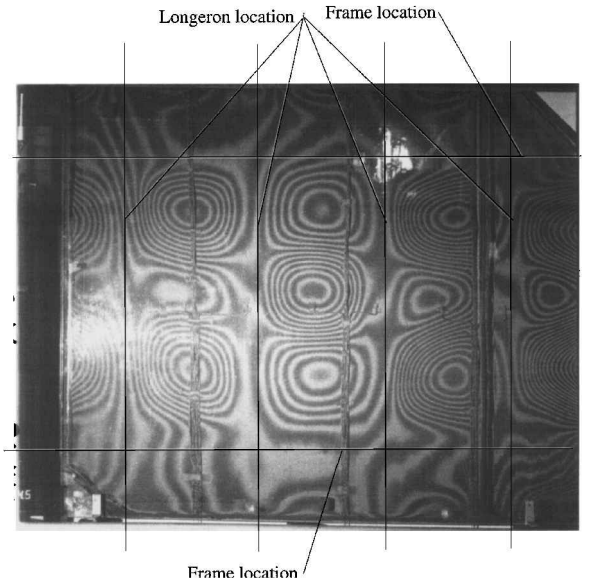

b) Applied compressive load of 44,000 lb (196 kN)

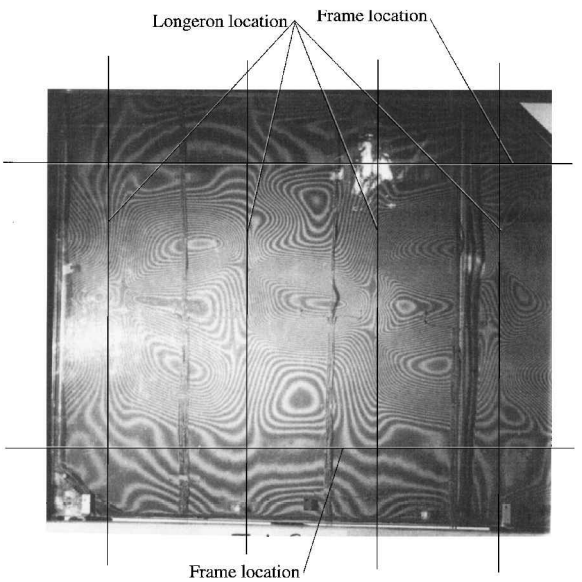

c) Applied compressive load of 85,000 lb (378 kN)

Fig. 4 Out-of-plane deformations.

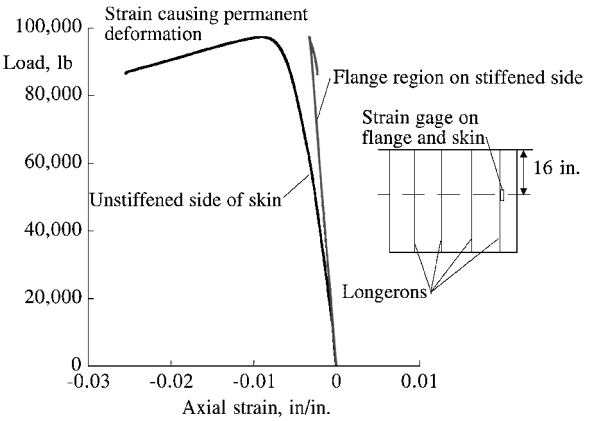

a) Measured strains

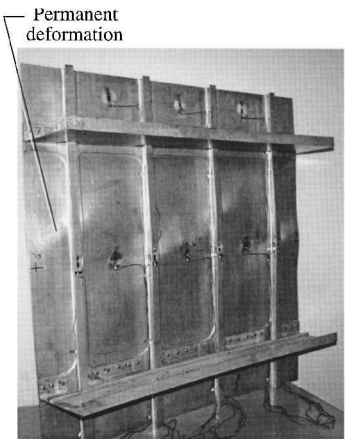

b) Panel after testing

Fig. 5 Permanent deformations.

rotations restrained and with loaded-end rotations unrestrained, respectively. The lowest predicted value of the buckling loads corresponds to mode shapes with buckles in the outer thin-skin regions. Higher values of buckling loads correspond to buckling in the thin-skin regions between frames and longerons.

End-shortening results for the test panel, for the analysis of a geometrically perfect panel, for the analysis of a geometrically imperfect panel using three types of boundary conditions, and for the geometrically imperfect panel with longeron-to-frame clips are shown in Fig. 6. The predicted stiffness of the perfect panel is only shown for loads less than 40,000 lb (177 kN) because of an inability to obtain convergence for higher load levels. The experimentally determined stiffness is approximately 12% less than the stiffness calculated by the analyses. The analyses of the geometrically imperfect panels resulted in a stiffness prediction that is the same as that calculated for the geometrically perfect panel, indicating that the global stiffness of the panel is unaffected by the assumed geometric imperfection. Similarly, no difference is seen between the end-shortening predictions for the different boundary conditions. Added restraints connecting the frame to the longeron at each mousehole do not affect the global stiffness of the panel.

Axial strains measured in the test panel and those predicted by analysis of the geometrically perfect panel and of the geometrically imperfect panels are shown in Fig. 7 for strain gauges located 2 in. (5.08 cm) from the top of the panel. Boundary conditions have little effect on the strains so that results for the boundary conditions with rotations of the longerons permitted at the loaded ends are presented in Figs. 8–14. Results are shown for back-to-back strain gauges midway between the center two longerons and on the flange region of the two center longerons. Experimental and analytical results for loads less than 40,000 lb (177 kN) are shown in Fig. 7a for the test panel, for a geometrically perfect panel, and for a geometrically imperfect panel without longeron-to-frame connections.

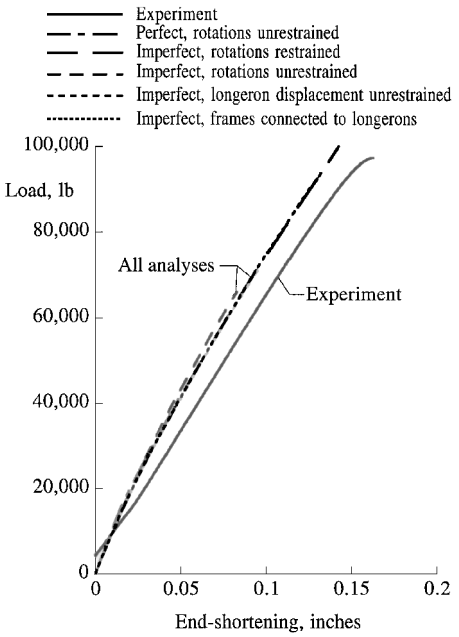

Fig. 6 End-shortening results as a function of applied load.

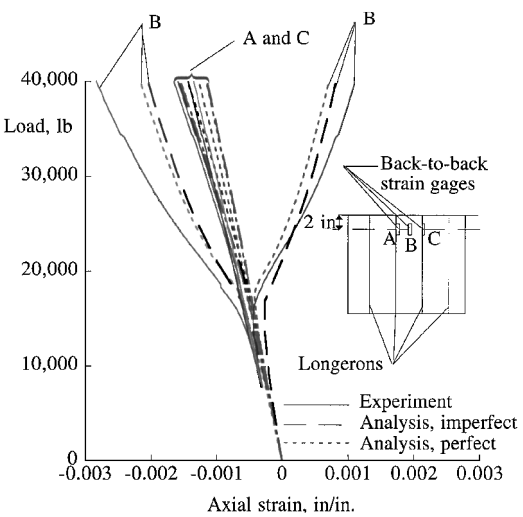

a) Strain gauge results in top center bay for load less than 40,000 lb (177 kN)

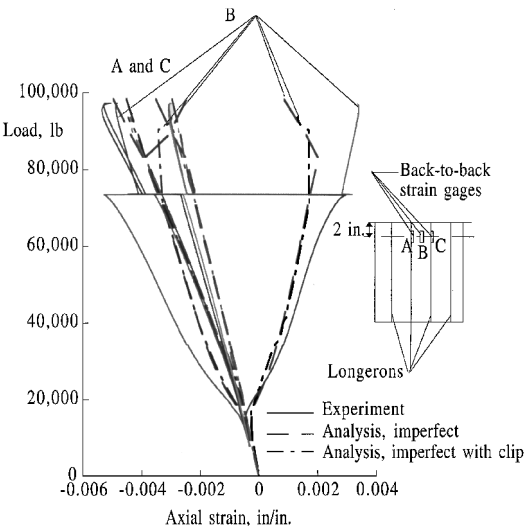

b) Strain gauge results in top center bay for load less than 100,000 lb (445 kN)

Fig. 7 Axial strain near loaded edge.

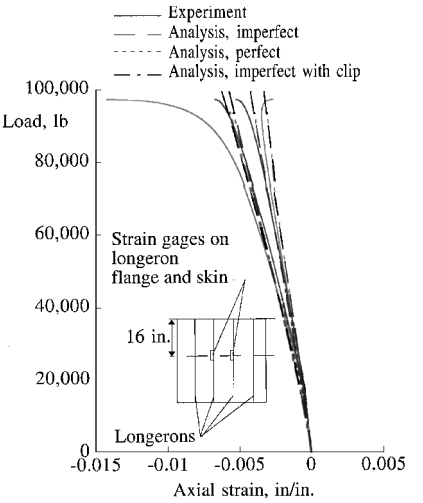

a) Strains in central longerons

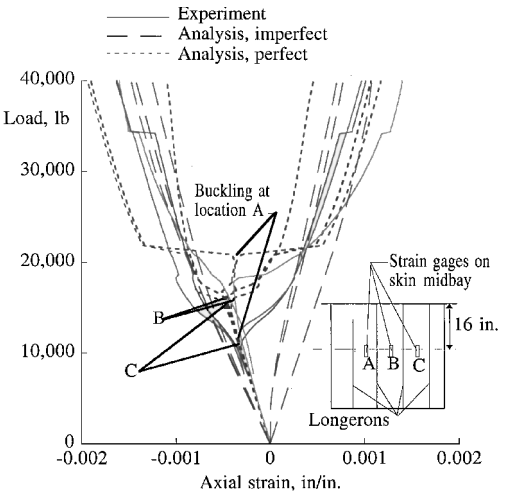

b) Midbay strains for load less than 40,000 lb (177 kN)

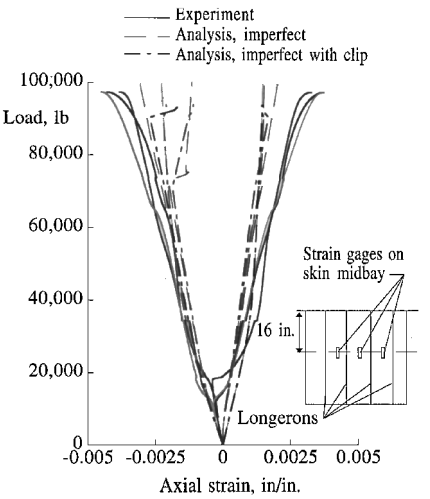

c) Midbay strains for load less than 100,000 lb (445 kN)

Fig. 8 Axial strain along panel centerline.

Midbay strain gauges (labeled site B in the figure) indicate that buckling occurs at a load of approximately 17,000 lb (75 kN) in this skin bay, which is consistent with the results from the analyses of the geometrically perfect and imperfect panels. Results that are approximately linear from the strain gauges at the stiffeners indicate that buckling does not occur at sites A and C. Test and analysis show the same trends in strains.

Results for loads up to 100,000 lb (445 kN) are shown in Fig. 7b for the test panel, a geometrically imperfect panel without

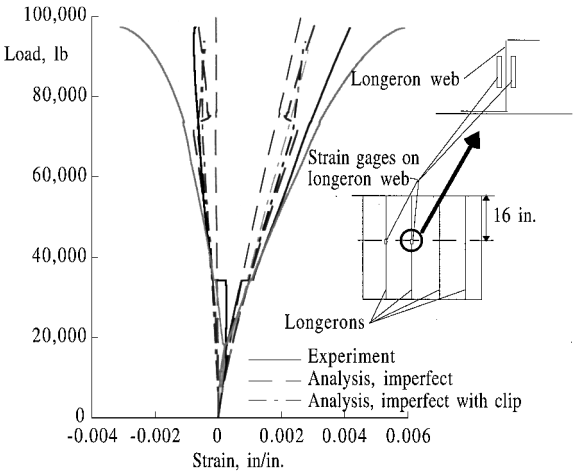

Fig. 9 Longeron rolling.

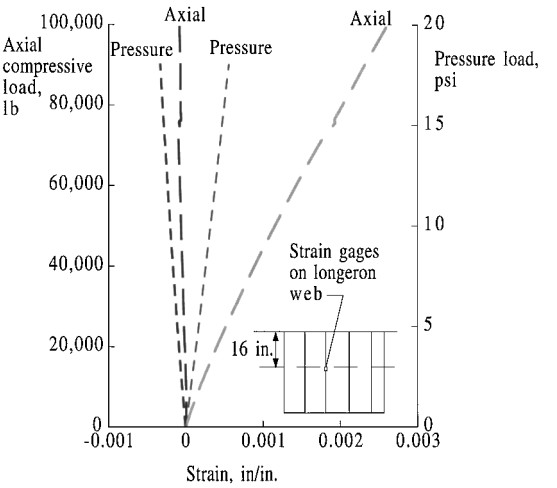

Fig. 12 Strains in longerons caused by compression or pressure.

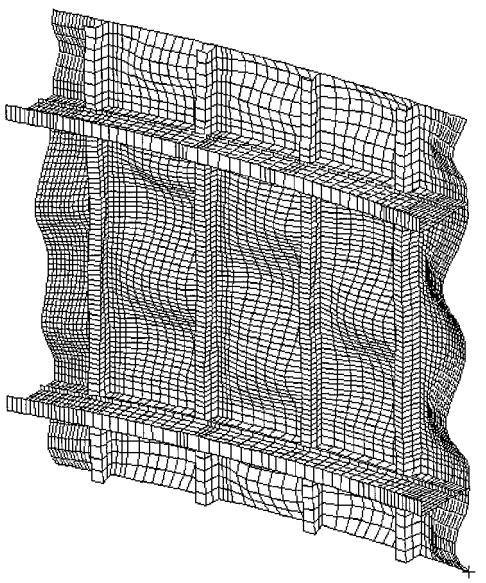

Fig. 10 Displacement pattern of axially compressed panel at 85,000 lb of load.

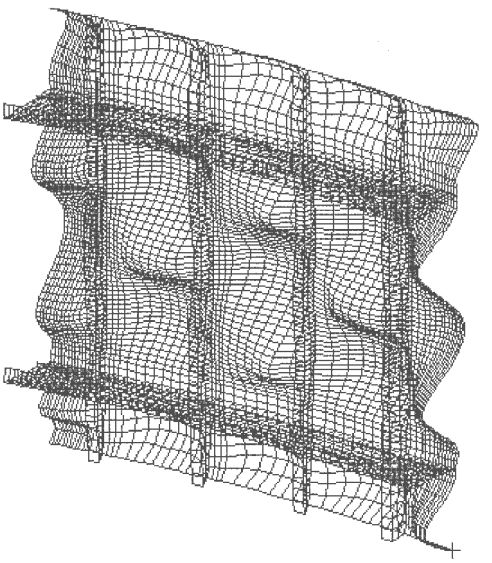

Fig. 13 Strains in longerons caused by pressure load with and without axial compressive load.

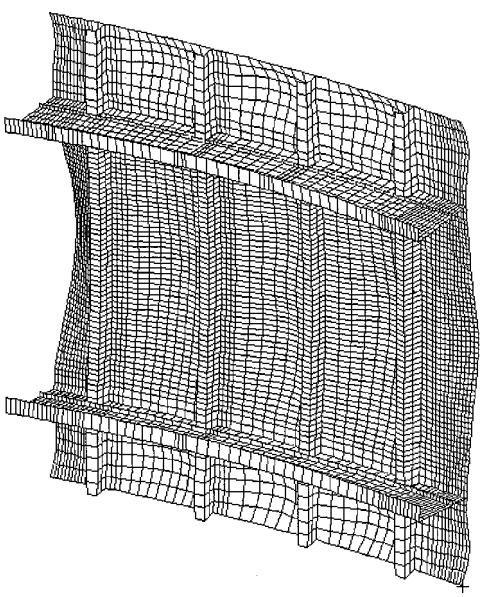

Fig. 11 Displacement pattern of internally pressurized panel at 18 psi of load.

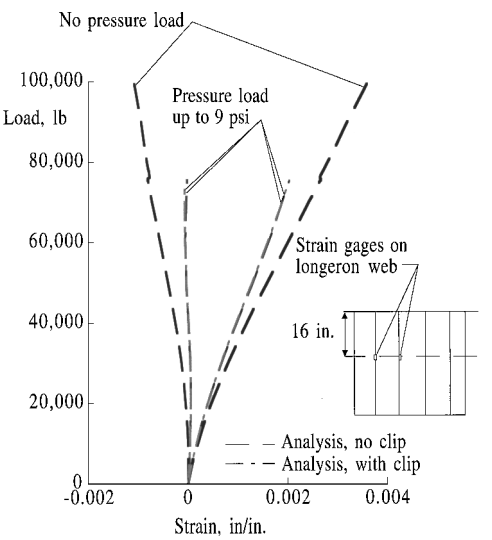

Fig. 14 Displacement pattern of panel subjected to 74,000 lb (329 kN) of axial compressive load and 9 psi internal pressure load.

longeron-to-frame connections, and for a geometrically imperfect panel with longeron-to-frame connections. Nine lines are shown in Fig. 7b, and none are linear; all indicate that the panel behavior after buckling is complicated with numerous buckling modes affecting the data in both test and analysis. Midbay strains from test and analysis indicate a greater difference between back-to-back strains for the test than for the analysis. In addition, a snap-through response (instantaneous change in deformation shape) occurs, at a load of 73,610 lb (327 kN) in the test, but no snap-through response occurs in the analyses. However, little difference can be seen between the results from the analysis of the panel without longeron-to-frame connections and for the panel with longeron-to-frame connections. Experimental and analytical results indicate that the axial strains in the longerons are linear for loads less than approximately 90,000 lb (400 kN). Test results agree well with predictions for locations A and C. Analysis does not predict the snap-through response phenomenon indicated at location B, but buckling behavior is still predicted accurately. Adding the connection between the longerons and the frames has little effect on the behavior of this panel skin bay.

Axial strains measured in the test panel and predicted by the analysis for a geometrically perfect panel and a geometrically imperfect panel are shown in Figs. 8 and 9 for strain gauges located at the axial centerline of the panel. Measured and predicted axial strains at the flanges of the central two longerons are shown in Fig. 8a. These strains are linear for loads less than approximately 80% of the failure load, and analysis results agree well with test results for the geometrically perfect panel analysis and the two geometrically imperfect panel analyses. Measured and predicted axial midbay strains between the longerons are shown in Figs. 8b and 8c. Midbay strain gauges indicate that buckling occurs at a load of approximately 12,000 lb (53 kN) in all three central bays of the test panel. Analysis of the geometrically perfect panel indicates that buckling occurs at a load of approximately 16,000 lb (71 kN) in two bays and at approximately 20,000 lb (89 kN) in the third bay. Buckling loads in these bays of the geometrically imperfect panel are not predicted because the skin in these bays is assumed to have a buckled deformation shape prior to loading. There is little difference between the predictions for the panel with longeron-to-frame connections and the panel without these connections. Test results agree well with predictions. For a load of 98,000 lb (436 kN), the axial strains in the panel range from -0.0005 to -0.0075 in./in. whether the longeron-to-frame connections are present or not.

The strains in the web of the longerons are shown in Fig. 9. Surface strains in the longeron perpendicular to the skin can be used to evaluate rolling or rotation of the longerons. The large difference between the strains on the front and back surface of the longeron web of the test panel indicates rolling of the longeron. Similarly, the difference between predicted surface strains indicates that the analysis predicts rolling of the longeron at the axial center of the panel. The similarity of these strains for the test and for both analyses indicates that rolling of the longerons is predictable. However, more rolling is indicated by the test data than by the analysis results for the test panel. A comparison between the analytical results for the panel with no longeron-to-frame connection and for the panel with these connections indicates that the longerons roll at the center of the panel even if they are supported at the frame locations. The frames are 24 in. (0.61 m) apart, and this distance is too great to reduce significantly the rolling of the longerons halfway between the frames.

The predicted deformation shape of the geometrically imperfect panel without longeron-to-frame connections and subjected to a load of approximately 85,000 lb (378 kN) is shown in Fig. 10. The deformations are amplified by a factor of 10 in the figure to make them more visible. The skin deformation is much greater than the deformation of the longerons so that rolling of the longerons cannot be seen in the figure. The out-of-plane deformations shown in Fig. 10 are similar to the pattern of the deformations shown in Fig. 4c, which shows the out-of-plane deformations of the test panel at a load of 85,000 lb. Out-of-plane deformations for the panel with longeron-to-frame connections are very similar to those of the panel without these connections.

Internal Pressure

A panel with and without longeron-to-frame connections was analyzed with an applied internal pressure load of 18 psi. The deformations from these analyses are almost identical, but they are different from the deformations of the panel subjected to the axial compressive load. The deformation pattern for the pressure-loaded panel is shown in Fig. 11. The deformations are amplified by a factor of 10 in the figure to make them more visible. The most significant deformation is at the unsupported edges. Less deformation occurs for the pressure-loaded panel than for the axially loaded panel. The effect of the pressure load on longeron rotation is determined by examining the surface strains on the web of the longerons. These strains at the centerline of one longeron are shown in Fig. 12 for the axially compressed panel without longeron-to-frame connections and for the pressure-loaded panel with and without longeron-to-frame connections. The scale on the left side of the figure shows axial compressive load and applies to the long dash curve in the figure. The scale on the right side of the figure shows the pressure load and applies to the short-dash curves in the figure. The pressure loading does not induce significant longeron rolling. The maximum surface axial strain is 0.002 in./in. for assumed loads up to 18 psi.

Combined Loads

A combination of an axial compressive load and an internal pressure load was analytically applied to a panel with longeron-to-frame connections and to a panel without longeron-to-frame connections. The maximum applied pressure load is 9 psi, and the maximum axial compressive load is 74,000 lb (329 kN). The strains in a longeron web for these two panels and for the panel with only an axial compressive load are shown in Fig. 13. The difference in the surface strains indicates that the longerons roll. However, a comparison between the strains for a panel loaded only by axial compression and for a panel subjected to combined loads indicates that the longerons in the pressure-loaded panel roll less than the longerons in the combined-load panel when subjected to the same axial compressive load. The deformation shape of the geometrically imperfect panel without longeron-to-frame connections is shown in Fig. 14. For a load of 98,000 lb (436 kN), the axial strains in the panel range from -0.0005 to -0.0075 in./in. whether the longeron-to-frame connection is present or not.

Conclusions

An aluminum panel representative of an aircraft fuselage structure was loaded experimentally in axial compression and analyzed for both axial compression and internal pressure loads. The panel was fabricated with the longerons and skin cut from one piece of 7050-T7451 aluminum to verify that integral stiffeners can be manufactured within tolerances using this material. The panel test results verified that an integrally stiffened panel can support sufficient loads to be useful as an aircraft structural part with no fasteners to attach the longerons to the skin. The panel failed as a result of permanent deformations without any cracks or broken components. The panel withstood 97,200 lb (432 kN) of load and 30,000 psi of stress.

Analytical results agree well with test data, and these results accurately predicted out-of-plane deformations, longeron rolling, and surface strains. Analytically varying boundary conditions on the unloaded edges of the panel had little effect on panel behavior. The addition of connections or clips between the frames and the longerons at each longeron-to-frame intersection had almost no effect on the panel behavior in terms of displacements, stiffness, or strains for any of the loading conditions or boundary conditions considered. The frame spacing of 24 in. (0.61 m) appears to be too long for the longeron-to-frame clips to affect or prevent the rolling of the longerons halfway between frames.

Internal pressure loads up to 18 psi induce strains of less than 0.002 in./in., which would not alone cause failure. The pressure-loaded panel displays less longeron rolling than the axially compressed panel. A combination of internal pressure and axial compressive loads induces less strain than the axial compressive

load acting alone, and the combined loads induce a different deformation pattern than either load acting alone.

The integral-stiffened structure was able to support sufficient load to warrant further consideration of this structural concept to help achieve the goal of reducing part count and cost associated with aircraft manufacturing.

References

[1]Rankin, C. C., Brogan, F. A., Loden, W. A., and Cabiness, H. D., "STAGS User Manual, Version 3.0," Lockheed Martin Missiles and Space Co., Inc., Rept. LMSC P032594, Palo Alto, CA, March 1999.

[2]Rankin, C. C., and Brogan, F. A., "The Computational Structural Mechanics Testbed Structural Element Processor ES5: STAGS Shell Element," NASA CR 4358, May 1991.

[3]Riks, E., "Some Computational Aspects of the Stability Analysis of Nonlinear Structures," *Computer Methods in Applied Mechanics and Engineering*, Vol. 47, No. 3, 1984, pp. 219–259.

[4]Riks, E., "Progress in Collapse Analysis," *Journal of Pressure Vessel Technology*, Vol. 109, No. 1, Feb. 1987, pp. 33–41.

[5]Young, R. D., and Rankin, C. C., "Modeling and Nonlinear Analyses of a Large-Scale Launch Vehicle Under Combined Thermal and Mechanical Loads," *Proceedings of the 37th Structures, Structural Dynamics, and Materials Conference*, AIAA, Washington, DC, 1996, pp. 2023–2033.